Relaxation dynamics in a Fe7 nanomagnet

Relaxation dynamics in a Fe_7 nanomagnet

E. Garlatti,[1,2] S. Carretta,[2] P. Santini,[2] G. Amoretti,[2] M. Mariani,[3,4] A. Lascialfari,[1,3] S. Sanna,[3] K. Mason,[5] J. Chang,[5] P. Tasker,[5] and E. K. Brechin[5]

[1]*Dipartimento di Fisica, Università degli Studi di Milano, Via Celoria 16, 20133 Milano, Italy*
[2]*Dipartimento di Fisica e Scienze della Terra, Università di Parma, Viale G.P. Usberti 7/A, 43124 Parma, Italy*
[3]*Dipartimento di Fisica, Università di Pavia, Via Bassi 6, 27100 Pavia, Italy*
[4]*Dipartimento di Fisica e Astronomia (DIFA), Università di Bologna, Viale Berti-Pichat 6/2, 40127 Bologna, Italy*
[5]*School of Chemistry, The University of Edinburgh, West Mains Road, Edinburgh, EH9 3JJ, United Kingdom*

(Received 11 July 2012; published 13 February 2013)

We investigate the phonon-induced relaxation dynamics in the Fe_7 magnetic molecule, which is made of two Fe^{3+} triangles bridged together by a central Fe^{3+} ion. The competition between different antiferromagnetic exchange interactions leads to a low-spin ground state multiplet with a complex pattern of low-lying excited levels. We theoretically investigate the decay of the time correlation function of molecular observables, such as the cluster magnetization, due to the spin-phonon interaction. We find that more than one time contributes to the decay of the molecular magnetization. The relaxation dynamics is probed by measurements of the nuclear spin-lattice relaxation rate $1/T_1$. The interpretation of these measurements allows the determination of the magnetoelastic coupling strength and to set the scale factor of the relaxation dynamics time scales. In our theoretical interpretation of $1/T_1$ data we also take into account the wipeout effect at low temperatures.

DOI: 10.1103/PhysRevB.87.054409 PACS number(s): 75.50.Xx, 76.60.Es

I. INTRODUCTION

Molecular nanomagnets (MNMs) have attracted the attention of the scientific community in the field of low-dimensional magnetism both for their physical properties of fundamental interest and for the potential technological applications. They are characterized by strong exchange interactions within their magnetic core, consisting of 3d paramagnetic ions. Intermolecular dipolar interactions are instead very weak due to the presence of shells of organic ligands around the magnetic core of each molecule. Hence, bulk crystals behave like an ensemble of isolated and identical zeroth-dimensional magnetic units.

The envisaged technological applications based on MNMs go from high-density memory storage[1,2] and quantum information processing[3–6] to magnetocaloric refrigeration.[7,8] In addition, MNMs exhibit a wide range of intriguing quantum phenomena, such as quantum tunneling of the magnetization,[9–11] decoherence,[12,13] or quantum entanglement between distinct cores.[14–17] MNMs also present great advantages from the standpoint of theoretical modeling. Indeed, it has been demonstrated that the effective spin Hamiltonian is a powerful model to describe magnetic properties of these clusters.[18] It is important to note that this model can often be simulated exactly with analytical or numerical methods. Moreover, molecular structures of MNMs can be controlled by synthetic chemistry in order to tune the resulting magnetic properties.

A new route in molecular magnetism is based on magnetically frustrated MNMs. In fact, geometrical magnetic frustration is at the origin of many exotic phenomena.[19] It occurs when the presence of competing interactions forbids the simultaneous minimization of all individual two-spin terms,[20] as happens in an AF-coupled system of three spins in a triangle. MNMs with competing antiferromagnetic interactions can display geometrical frustration, but the effects of frustration on their static and dynamical properties are still largely unexplored. They also represent ideal systems to study the interplay between frustration and quantum effects due to their zeroth-dimensional character.[21] Magnetically frustrated MNMs have also been proposed for technological applications in magnetocaloric refrigeration,[22] due to their large energy degeneracies and hence large field-induced entropy variations.

In the present paper we investigate the spin dynamics of an Fe_7 molecular nanomagnet, whose magnetic core consists of seven AF-coupled Fe^{3+} ions arranged on two corner-sharing tetrahedra[23] (see Fig. 1). Its structure is similar to that of a piece bulk pyrochlore, in which geometrical frustration leads to peculiar magnetic properties. Frustration effects in MNMs have been theoretically predicted in a similar system, Ni_7,[24] which displays a large ground state degeneracy and unusual static and dynamical magnetic properties. A great advantage of these two clusters is the relatively small Hilbert space compared to other frustrated clusters. Indeed, this makes (virtually) exact calculations feasible. The possibility to neglect the effects of anisotropies on Fe^{3+} ions makes Fe_7 even more appealing than Ni_7 in order to study frustration-induced properties. Unfortunately, the magnetic core of the Fe_7 cluster shows small structural distortions (the upper and the lower triangles are not exactly equilateral and they are slightly different from each other). Even if these distortions lead to a removal of frustration, there are still many competing AF interactions leading to a low-spin ground state multiplet with a complex pattern of low-lying excited levels.[23] This yields a multiple-time-scale relaxation dynamics at low temperatures. Such behavior is one of the main features we expect in a frustrated MNM.[24] Conversely, single-molecule magnets like Fe_8[25] and AF rings like Cr_8[26] are characterized by a single dominant relaxation time.

Phonon-induced relaxation dynamics in MNMs can be probed by the proton spin-lattice relaxation rate $1/T_1$, measured by nuclear magnetic resonance (NMR).[25,27] In fact the interpretation of ^{1}H nuclear magnetic resonance measurements allows the determination of the coupling strength of the

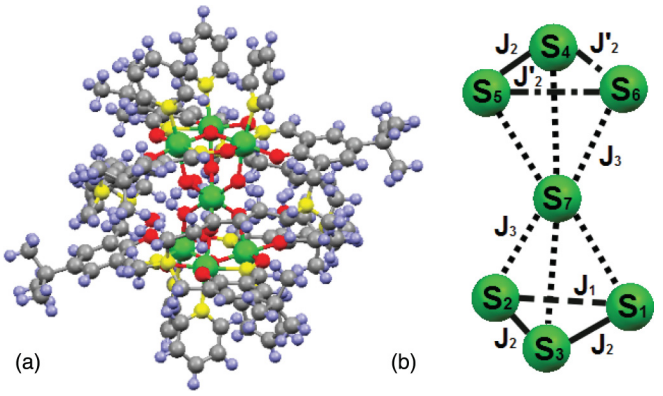

FIG. 1. (Color online) (a) Molecular structure of Fe_7 (red: O, cyan: H, gray: C, yellow: N). The large green spheres are Fe^{3+} ions. (b) Magnetic core of Fe_7. Lines represent exchange interactions; the four different exchange parameters J_1 (dashed line), J_2 (solid line), J_2' (dash-dotted line) and J_3 (dotted line) reflect the different Fe-Fe superexchange paths (Ref. 23).

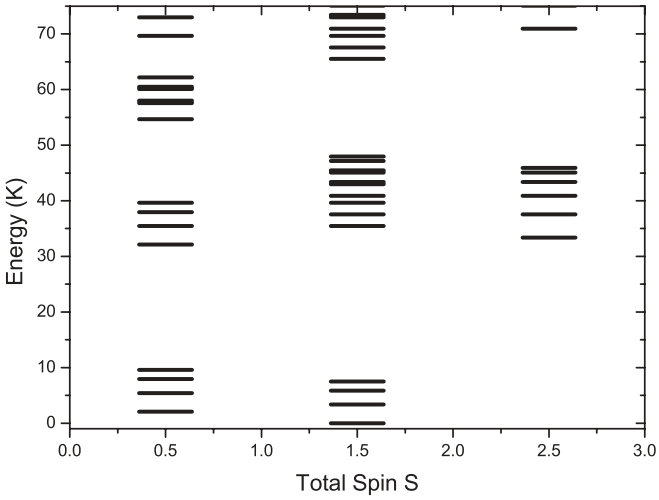

FIG. 2. Exchange energy of the lowest total spin multiplets calculated with the spin Hamiltonian (1) and $J_1 = 83$ K, $J_2 = 91$ K, $J_2' = 92$ K, and $J_3 = 77$ K (Ref. 23). The ground state energy is set to zero.

magnetoelastic interaction and to calculate, for instance, magnetization relaxation times. In this work we have measured the temperature dependence of $1/T_1$ for two different values of the applied magnetic field. NMR measurements on MNMs are often affected by the so-called wipeout effect:[28] At low temperatures it is possible to have an NMR signal loss, due to the enhancement of the protons transverse relaxation rate $1/T_2$ over the limit of the experimental signal detection capability. As a consequence, not all the protons contribute to the molecular $1/T_1$. Within our theoretical framework it is possible to reproduce this wipeout effect by identifying which protons are probed by NMR.

II. THEORETICAL MODEL

The magnetic properties of the Fe_7 cluster can be described by the following spin Hamiltonian:

$$\mathcal{H} = \sum_{i>j=1}^{N} J_{ij}\mathbf{s}_i \cdot \mathbf{s}_j + g\mu_B \mathbf{B} \cdot \sum_{i=1}^{N} \mathbf{s}_i \qquad (1)$$

($s_i = 5/2$ for Fe^{3+} and $N = 7$). The first term represents the isotropic Heisenberg exchange interaction and the last one is the Zeeman coupling to an external magnetic field ($g = 2$ for Fe^{3+}). Fe^{3+} ions are characterized by a half-filled d-electron shell, thus anisotropic exchange and crystal field interactions are small and can be neglected. The exchange parameters in Eq. (1) have been determined by magnetic measurements of susceptibility and magnetization[23] (see the caption of Fig. 2). To explain the observed magnetic behavior, four distinct exchange couplings are needed, reflecting the small structural distortions in the cluster [for a schematic representation of exchange interactions see Fig. 1(b)].

We have found that the energy spectrum of Fe_7 must have precise characteristics in order to reproduce the features of the magnetic data.[23] As we will show in the next section, these characteristics are also responsible for the multiple-time-scale relaxation dynamics of the cluster. First of all, the measured low-T values of χT are smaller than those corresponding to an isolated $|S = 3/2\rangle$ multiplet, but higher than those of an isolated $|S = 1/2\rangle$ doublet. In addition, the $\chi T(T)$ curve at low temperature has a nearly linear behavior. These features indicate the presence of a ground state with low spin S and of several low-lying excited states. In addition, the Mvs B curve at low temperature keeps the values of $3\mu_B$, corresponding to the $|S = 3/2\rangle$ ground state, up to very high fields.[23] Therefore we can conclude that the energy spectrum has a low-spin ground state $|S = 3/2\rangle$ with a very small gap (of a few K) with the first excited doublet $|S = 1/2\rangle$ and with the low-lying $|S = 3/2\rangle$ excited multiplets and a very large gap (higher than 30 K) with the first excited $|S = 5/2\rangle$ multiplet.

The Fe_7 magnetic data can be acceptably reproduced in several regions of the parameter space (see supplementary information in Ref. 23 for further details), consistent with the above-mentioned conditions for the energy spectrum. As we pointed out in the supplementary information, there is only one region satisfying the magnetostructural correlations,[29] to which our final set belongs. The energy spectrum calculated with this set of parameters is reported in Fig. 2. The competition between the strong AF interactions leads to a $|S = 3/2\rangle$ ground multiplet with several low-lying excited levels. Figure 3 shows the calculated magnetic field dependence of the lowest lying energy levels.

Molecular observables are affected by interactions of spins with other degrees of freedom, like phonons, which behave as a heat bath. They cause decoherence of the time evolution of the observables leading to relaxation dynamics, that can be described through the formalism of rate (master) equations.[25] Since we focus on time scales τ much longer than the free evolution periods of the system [$2\pi\hbar/(E_s - E_t)$, with E_s and E_t eigenvalues of Eq. (1)], the secular approximation allows us to decouple the time evolution of the diagonal elements of the density matrix $p_s(t) = \rho_{ss}(t)$ from that of the off-diagonal elements $\rho_{st}(t)$ with $s \neq t$. In the frequency-domain picture, this corresponds to a separation between quasielastic and inelastic spectral contributions. To study the relaxation dynamics of Fe_7, we focus on the quasielastic components which can be probed by NMR measurements.[25,30] Within

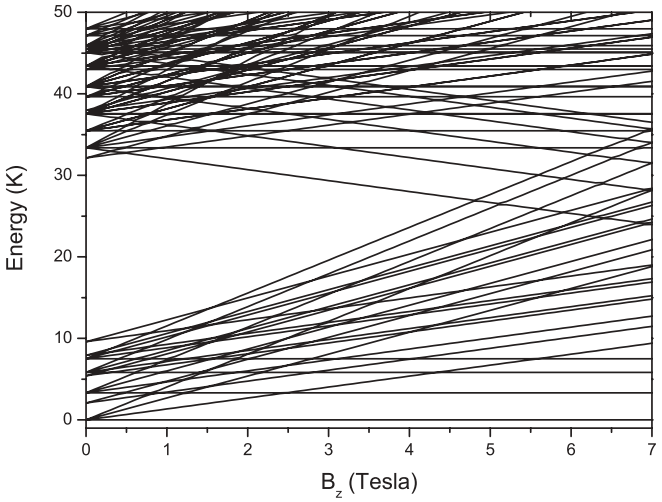

FIG. 3. Magnetic field dependence of the lowest lying energy levels of Fe_7 calculated with equation (1). The magnetic field is applied along the z axis. The ground state energy is set to zero for each value of B_z.

this framework, the coarse-grained time evolution of the population p_s is given by the master equations:

$$\dot{p}_s = \sum_t W_{st} p_t, \tag{2}$$

where W_{st} are the elements of the rate matrix $\mathbb{W}$, i.e., the probability per unit time that a transition between the eigenstates $|t\rangle$ and $|s\rangle$ is induced by the phonon heat bath. The precise form of the rate matrix depends on the details of the spin-phonon interaction mechanism. Here we have assumed that each ion experiences a spherically symmetric magnetoelastic coupling, due to crystal fields modulations induced by phonons, which are described by a Debye model. Thus we can write the transition rates as[31]

$$W_{st} = \gamma \pi^2 \Delta_{st}^3 n_{ph}(\Delta_{st}) \times \sum_{i,j=1}^{N} \sum_{q_1,q_2=x,y,z} \langle s|O_{q_1,q_2}(\mathbf{s}_i)|t\rangle \langle s|O_{q_1,q_2}(\mathbf{s}_j)|t\rangle^*, \tag{3}$$

where $n_{ph}(x) = (e^{\hbar x/k_B T} - 1)^{-1}$, $\Delta_{st} = (E_s - E_t)/\hbar$, and $O_{q_1,q_2}(\mathbf{s}_i) = (s_i^{q_1} s_i^{q_2} + s_i^{q_2} s_i^{q_1})/2$ are the quadrupolar operators. The coupling strength γ is the only free parameter and it can be determined from NMR experimental data.[32] The relaxation dynamics towards equilibrium can be described in terms of the equilibrium dynamical correlation functions between the fluctuations of molecular observables, $\mathcal{S}_{\mathcal{P},\mathcal{Q}}(t) = \langle (\mathcal{P}(t) - \mathcal{P}_{eq})(\mathcal{Q}(t) - \mathcal{Q}_{eq})\rangle$. In the theoretical framework given by equations (2) and (3), the Fourier transform of the correlation function can be expressed as a sum of Lorentzians:[25]

$$\mathcal{S}_{\mathcal{P},\mathcal{Q}}(\omega) = \sum_{i=1}^{n} A(\lambda_i, T, B) \frac{\lambda_i(T,B)}{\lambda_i(T,B)^2 + \omega^2} \tag{4}$$

(n is the dimension of the Hilbert space). The relaxation rates λ_i are the eigenvalues of $-\mathbb{W}$ and they are the inverse of the characteristic relaxation times $\tau_{\rm rel}^{(i)} = 1/\lambda_i$. The weights $A(\lambda_i, T, B)$ of each rate λ_i are calculated by equations (2) and (3), as explained in Refs. 25 and 33.

III. RELAXATION DYNAMICS

Within the theoretical framework illustrated in Sec. II, we can investigate the relaxation dynamics of the Fe_7 cluster by applying equation (4) to the most interesting observables. Here we focus on the relaxation of the cluster magnetization ($\mathcal{P} = \mathcal{Q} = \mathcal{M} = \sum_i s_i^z$) and on single-site spin observables s_i^z, where z is the direction of the external field. In Fig. 4 we report the calculated relaxation rates spectra of $\mathcal{M}$ as a function of temperature for three different values of the applied fields (0.01 T and the two fields used in NMR measurements).

The only free parameter of the model, the spin-phonon coupling strength γ, has been determined from the analysis of $1/T_1$ NMR data, that will be discussed in the next section. It is worth stressing that this parameter merely fixes the overall scale factor of the relaxation dynamics time scales (a change of γ only leads to rigid vertical shifts in Figs. 4 and 5), whereas the temperature and field dependence of the relaxation rates comes directly from the calculations.

The rates $\lambda_i(T)$ having appreciable weight in the spectra are roughly in the range 10^{-9}–10^{-1} THz up to $T = 30$ K, corresponding to relaxation times between 1 ms and 10 ps. The relaxation dynamics become faster as the applied magnetic field increases, especially at low T. The most interesting feature of the Fe_7 relaxation dynamics is that several rates have appreciable weights, even at rather low temperatures. Conversely, in most MNMs a single rate dominates at low temperature. This multiple-time-scale dynamics is a peculiar characteristic of Fe_7, due to the effects of AF competing interactions on the energy spectrum. Since there is a complex pattern of low-lying excited levels, the spin-phonon interactions can induce many relaxation processes, with different paths and different characteristic times $\tau_{\rm rel}^{(i)}$. For different values of the applied field, we have analyzed the dominant relaxation processes at low temperatures by inspecting the eigenvectors of Eq. (2) and the matrix elements of Eq. (3). In fact, the former give information about the starting and the final levels of the processes and the latter are the transition probabilities. In small field (Fig. 4 top panel) we have found that the two dominant relaxation rates at $T \lesssim 2.5$ K follow the Arrhenius law $\lambda = \lambda_0 \exp(-\Delta/k_B T)$, where the amplitude λ_0 sets the time scale and reflects the magnetoelastic coupling strength γ, and Δ/k_B is the height of the barrier hampering the relaxation of $\mathcal{M}$. These two relaxation processes involve levels of the ground state manifold $S = 3/2$ and of the lower-lying $S = 1/2$ and $S = 3/2$ multiplets. In fact, the dominant relaxation time has $\Delta/k_B \approx 5.8$ K and it corresponds to an Orbach process[34] involving the ground state and the third excited manifold with $S = 3/2$, which has energy ≈ 5.8 K in zero field (see Fig. 2). The second important relaxation process is characterized by a smaller energy barrier $\Delta/k_B \approx 4.4$ K and it involves levels belonging to the third excited multiplet with $S = 3/2$ and $E_3 = 3.3$ K and to the sixth excited one with $S = 3/2$ and $E_6 = 7.5$ K in zero field. At 2.5 K $< T <$ 4 K the rate corresponding to the slowest relaxation process follows an Arrhenius law with $\Delta/k_B \approx 35$ K. This corresponds to an Orbach relaxation process involving the first excited multiplet with $S = 1/2$ and energy $E_1 = 2.1$ K and the $S = 3/2$ multiplet lying at about $E_{13} = 37.5$ K in zero field (see Fig. 2). This process gives a very small contribution to the relaxation dynamics of the

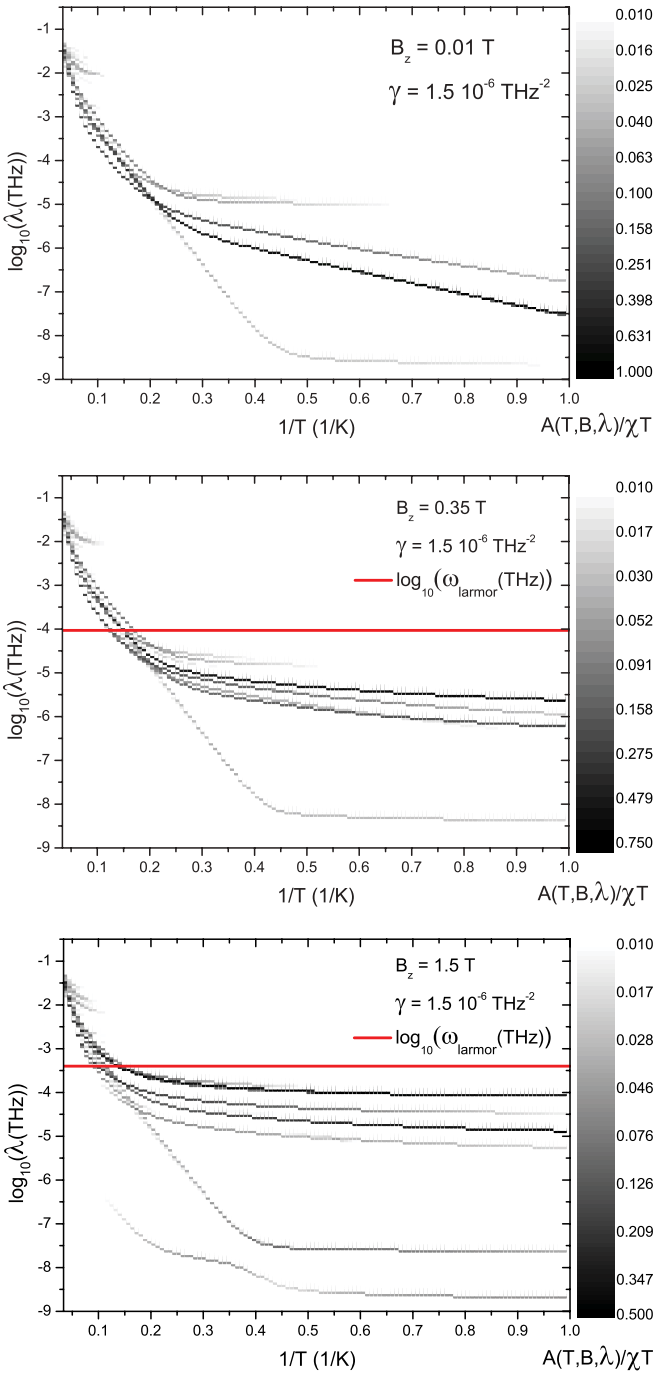

FIG. 4. (Color online) Calculated weights $A(\lambda_i, T, B)$ of the magnetization autocorrelation as a function of the inverse temperature for the three values of the applied magnetic field, $B = 0.01$ T, $B = 0.35$ T, and $B = 1.5$ T, respectively. The y axis is $\log_{10}(\lambda_i)$, the grayscale shows the weights $A(\lambda_i, T, B)/\chi T$. When ω_L (red line) intersects the rates λ_i with significant weight, $1/T_1$ displays a peak (see Fig. 6).

Fe_7 cluster, at odds with many MNMs where the slowest relaxation process is the dominant one. At higher temperatures several characteristic rates have an appreciable weight and the T dependence is not of the Arrhenius type.

By increasing the applied field (see Fig. 4 bottom panels), the multiple-times character of the relaxation dynamics becomes more pronounced. Moreover, the Arrhenius T-dependence of the dominant rates is lost even at low temperatures, while in most MNMs relaxation times at low temperatures follow the Arrhenius law even in a moderate applied magnetic field.[25,26] We have found that the two dominant relaxation rates at low temperatures correspond to direct processes involving levels of the ground multiplet, split by the Zeeman interaction with the field. The slowest relaxation process is still of the Arrhenius type and has a slightly larger weight. At $B = 1.5$ T an even slower relaxation process occurs, but it doesn't follow the Arrhenius law. We have also calculated the magnetic field dependence of the relaxation rates at $T = 1$ K, reported in Fig. 5. We have confirmed that the multiple-time-scale dynamics at low temperature is still present even with high applied magnetic fields (e.g., up to $B = 6$ T as shown in Fig. 5), with the two dominant relaxation rates increasing with the magnetic field.

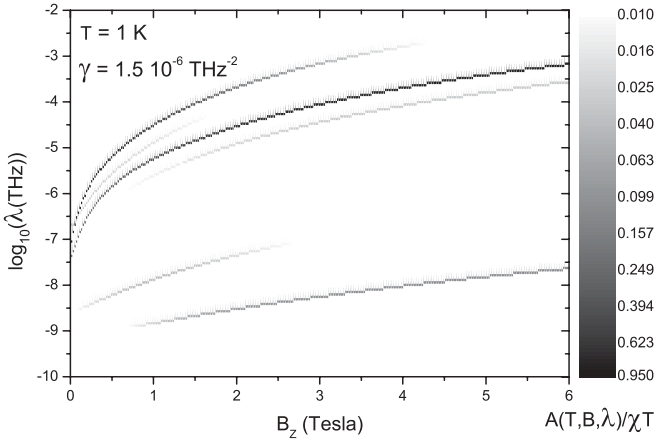

FIG. 5. Calculated weights $A(\lambda_i, T, B)$ of the magnetization autocorrelation as a function of the applied magnetic field at $T = 1$ K. The y axis is $\log_{10}(\lambda_i)$, the grayscale shows the weights $A(\lambda_i, T, B)/\chi T$.

We have verified that the multiple-time-scale relaxation dynamics is found also using sets of exchange parameters belonging to other regions of the parameters space, where it is possible to find acceptable fits of Fe_7 susceptibility and magnetization.[23] In fact, as already mentioned in Sec. II, the characteristics that the energy spectrum must have in order to reproduce the magnetic data are also responsible for the multiple-time-scale relaxation dynamics. Indeed, the two dominant frequencies in the spectrum of fluctuations of the cluster magnetization correspond to relaxation processes involving levels of the ground state manifold $S = 3/2$ and of the low-lying multiplets. We can therefore conclude that the multiple-time-scale dynamics does not depend on the specific choice of the parameter set used to interpret magnetic data.

IV. NMR EXPERIMENTS

The phonon-induced relaxation dynamics of the Fe_7 cluster has been probed by NMR. The theoretical model reported in the previous sections depends on the single free parameter γ, the spin-phonon coupling strength, which fixes the scale factor of the relaxation dynamics time scales. This parameter can be determined from the interpretation of the proton spin-lattice relaxation rate $1/T_1$, obtained from NMR experiments.

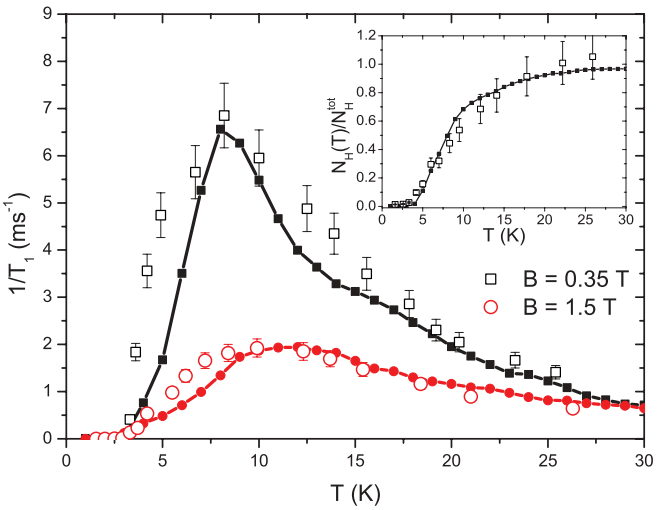

FIG. 6. (Color online) Scatter: ^{1}H NMR $1/T_1$ data on Fe_7 powders as a function of temperature at two different applied magnetic fields. Line and scatter: calculations exploiting equation (A5) and taking into account the wipeout effect. Inset: fraction of protons probed by NMR (scatter) deduced by the initial transverse nuclear magnetization at $B = 0.35$ T (see Sec. III). Line and scatter: fraction of protons taken into account in our calculations determined as described in Sec. IV.

In fact, thermal fluctuations of the electronic spins generate fluctuations in the local hyperfine field at the nuclear site, causing relaxation of the nuclear spins. Thus from ^{1}H NMR measurements it is possible to probe the relaxation dynamics of the cluster and determine the parameter γ.

We have measured the nuclear spin-lattice relaxation rate $1/T_1$ on a polycrystalline sample of Fe_7 as a function of temperature and for two values of the applied magnetic field, $B = 0.35$ T and $B = 1.5$ T. T_1 measurements have been performed by means of an Apollo-Tecmag FT pulsed NMR spectrometer. T_1 was determined after full irradiation of the nuclear absorption line using a comb of saturating $\pi/2$ pulses followed by a $\pi/2 - \pi/2$ solid-echo reading sequence. The $\pi/2$ length was kept between 2 and 2.5 μs. An effective value of T_1 was extracted by reading the renormalized nuclear magnetization curve $1 - M(t)/M(\infty)$ vs time at $1/e$, where $M(\infty)$ is the equilibrium value of M. Experimental results are shown in Fig. 6. The temperature dependence of $1/T_1$ shows a peak at about 8–10 K, whose height and position depends on the applied magnetic field. As shown in Fig. 6, the peak lowers and moves to higher temperatures by increasing the field. The quantity $M^H_{xy}(0)T$, determined at $B = 0.35$ T from the $M^H_{xy}(t)T$ relaxation curve, is proportional to the number of protons resonating at the irradiation frequency. Results as a function of temperature are shown in the inset of Fig. 6. $M^H_{xy}(0)T$ decreases by lowering the temperature due to the so-called wipeout effect, experimentally observed in other MNMs and qualitatively explained in Ref. 28.

The theoretical model illustrated in Sec. II and in the Appendix has been applied to the interpretation of ^{1}H NMR data on Fe_7. In order to reduce the computational effort, a truncation in the molecule Hilbert space is necessary to perform the diagonalization of the rate matrix $\mathbb{W}$. The reduction to the subspace spanned by the lowest total-spin manifolds (up to 200 K) allows us to calculate the temperature dependence of $1/T_1$ in the most interesting region, i.e., where it displays a peak, up to $T = 30$ K. Since $1/T_1$ measurements have been made on Fe_7 powders, to reproduce the experimental data we average over all the possible orientations of the applied external field.

From our theoretical model it is also possible to understand the origin of the peak in the temperature dependence of $1/T_1$, which has been experimentally observed in the Fe_7 nanomagnet as in other MNMs. First of all, we have also investigated the relaxation of single-site observables (s^z_i) and the decay of the hyperfine field fluctuations. We have found that the corresponding spectra are very similar to those of the cluster magnetization $\mathcal{M}$ in Fig. 4 and are characterized by the same dominant relaxation times. We can now exploit Eq. (4) to rewrite (for each hydrogen) the autocorrelation of the transverse components of the hyperfine field fluctuation [Eqs. 7 and 9] as a sum of Lorentzians evaluated at the Larmor frequency ω_L. In the case of homometallic AF rings only a single Lorentzian dominates the sum[25,30] and $1/T_1$ displays a peak at the temperature at which the relaxation rate of this Lorentzian matches ω_L. In the present case the relaxation dynamics is not mono-Lorentzian, but the different relevant rates are close to one another when they approach ω_L at T close to 10 K (see Fig. 4). Therefore, a single peak in the $1/T_1$ curve results also in the present case. Since the spin-phonon coupling strength γ sets the range of the characteristic relaxation times, it is possible to determine its value by fitting the position of the peak in $1/T_1(T)$.

As mentioned above, $1/T_1$ data on Fe_7 are also affected by the wipeout effect,[28] i.e., a gradual loss of the ^{1}H NMR signal intensity is observed upon decreasing the temperature. This signal loss is associated with the enhancement of the transverse relaxation rates of the probed protons over the limit fixed by the experimental setup; they become so fast that the transverse nuclear magnetization decays irreversibly before it can be observed in a pulsed NMR experiment. In our experimental conditions the minimum T_2 that we can measure in the investigated range of frequencies can be considered around 10–12 μs. We have taken into account the wipeout effect in our calculations by mimicking what actually happens in the NMR experiments. For each hydrogen in the molecule we use equations (A5) and (A6) to calculate $1/T_1$ and $1/T_2$ as a function of the temperature, the orientation, and the modulus of the applied magnetic field. Then, to determine the experimental $1/T_1$, i.e., averaged over all the protons in the molecule not affected by wipeout, we take into account only the hydrogen nuclei whose transverse relaxation rate is lower than a fixed threshold, $1/T_2 < 1/T_2^{\text{thresh}}$. Thus, in the calculation of $1/T_1$ we consider only the protons actually probed by NMR measurements. We let vary the T_2 threshold by an amount of 20%, with the aim of improving the final fits, thus obtaining $1/T_2^{\text{thresh}} = 86.6\ \text{ms}^{-1}$, corresponding to $T_2^{\text{threshold}} = 11$ μs, a value that falls perfectly in the experimentally estimated range. By fitting the peak position of $1/T_1(T)$ at $B = 0.35$ T, it is possible to determine the spin-phonon coupling strength, yielding $\gamma = 1.5 \times 10^{-6}\ \text{THz}^{-2}$. With the same parameter we have also reproduced the position and height of the peak in $1/T_1(T)$ at $B = 1.5$ T, confirming the correctness of the value of γ. Figure 6 demonstrates the good agreement between

the experimental results and our calculations. To check the reasonableness of our approach for mimicking the wipeout effect, we have estimated the temperature dependence of the fraction of probed hydrogens by measuring the transverse nuclear magnetization at time 0, obtained by the extrapolation at zero time of the transverse nuclear magnetization $M_{xy}^{H}(t)$ recovery curve (see the inset of Fig. 6). Indeed, the product $M_{xy}^{H}(0)T$ is proportional to the number of probed nuclei and can be compared with the number of ^{1}H included in our calculation by the method described above. These measurements have been performed at 0.35 T because wipeout is generally known to be stronger at small fields. The inset of Fig. 6 shows that our modeling captures the wipeout effect. It is worth noting that the conditions for the validity of the approximations underlying the present calculations (see the Appendix) are fulfilled except for the very low temperature region.

V. CONCLUSIONS

We have investigated the phonon-induced relaxation dynamics of the Fe_7 cluster, an excellent model system to study the effects of competing AF interactions on the spin dynamics of MNMs. We have found that several relaxation times $\tau_{\rm rel}^{(i)}$ contribute to the decay of the molecular magnetization even at low temperature. We have also verified that the multiple-times character of the relaxation dynamics is a direct consequence of the structure of the energy spectrum and that it is due to the topology of the competing AF interactions.

We have measured the temperature dependence of the spin-lattice relaxation rate $1/T_1$ by ^{1}H NMR measurements. The interpretation of these data has allowed us to determine the spin-phonon coupling strength γ and to set the scale factor of the relaxation dynamics time scales. By means of Redfield's approach[35] to the theory of relaxation processes, we have developed a model to calculate the nuclear spin-lattice relaxation rate $1/T_1$ taking into account also the wipeout effect. Our calculations are in very good agreement with experimental results.

In order to probe the multiple-times character of the relaxation dynamics of the Fe_7 cluster at low temperature, AC susceptibility experiments could be performed. In fact, the graph in Fig. 5 shows that the low temperature relaxation times can be detected by AC susceptibility measurements with very high frequency (of the order of 100 KHz) performed in small magnetic field, thus stimulating further experimental works on the cluster.

ACKNOWLEDGMENTS

This work was funded by the national PRIN-MIUR Project No. 2008PARRTS. F. Borsa is gratefully acknowledged for many discussions, suggestions, and a critical reading of the manuscript.

APPENDIX: NUCLEAR RELAXATION

Thermal fluctuations of the electronic spins are responsible for fluctuations in the hyperfine dipolar field and thus for the nuclear spin-lattice relaxation. The spin-lattice relaxation rate $1/T_1$ is therefore a powerful probe of the electronic relaxation times $\tau_{\rm rel}^{(i)}$ in MNMs. By the same density matrix formalism applied in Sec. II to the spin-phonon coupling, it is possible to describe the behavior of protons interacting with electronic spins, in the presence of an external magnetic field, i.e., ^{1}H NMR experiments. We follow the theory of relaxation processes of Redfield,[35] which is closely related to the treatment of relaxation due to Wangsness and Bloch,[36] to describe an ensemble of noninteracting protons in an external static magnetic field, coupled to the perturbative fluctuating field produced by electronic spins. This fluctuating field is different at each nuclear site, thus for each ^{1}H we have

$$\begin{aligned}\mathcal{H}_{\rm proton} &= \mathcal{H}_0 + \mathcal{H}_1(t) \\ &= -\gamma_N \hbar H_0 I_z - \gamma_N \hbar \mathbf{H}_{\rm hyp}(t)\cdot\mathbf{I}, \end{aligned} \tag{A1}$$

where H_0 is the static magnetic field along the z axis. The Larmor frequency is given by $\omega_L = \gamma_N H_0$, and $\mathbf{H}_{\rm hyp}(t)$ is the fluctuating hyperfine field

$$\mathbf{H}_{\rm hyp}(t) = -\hbar\gamma_e \sum_{i=1}^{N} \frac{1}{r_i^3}\left[\delta\mathbf{S}_i(t) - 3\mathbf{r}_i\left(\frac{\delta\mathbf{S}_i(t)\cdot\mathbf{r}_i}{r_i^2}\right)\right]. \tag{A2}$$

The index i labels the N magnetic ions, $\mathbf{S}_i$ represents their spin operators and $\mathbf{r}_i$ their distances from the proton, and $\delta\mathbf{S}_i(t) = \mathbf{S}_i(t) - \langle\mathbf{S}_i\rangle$. In Redfield's theory of relaxation processes[35] it is assumed that the ensemble average of the Hamiltonian $\mathcal{H}_1(t)$ vanishes, i.e., $\mathcal{H}_1(t)$ doesn't produce an average frequency shift. If this is not so, it's possible to redefine $\mathcal{H}_0$ in order to include the very-small average shift $\langle\mathcal{H}_1\rangle$. For this reason the Hamiltonian $\mathcal{H}_1(t)$ responsible for the nuclear relaxation in (A1) contains fluctuations $\delta\mathbf{S}(t)$ and not $\mathbf{S}(t)$.

By exploiting the secular and Markov approximations, the Redfield theory yields exponential time decays of the longitudinal and transverse nuclear magnetization with characteristic rates given respectively by[37]

$$\frac{1}{T_1} = \gamma_N^2[k_{xx}(\omega_L) + k_{yy}(\omega_L)], \tag{A3}$$

$$\frac{1}{T_2} = \frac{1}{2T_1} + \gamma_N^2 k_{zz}(0), \tag{A4}$$

where $k_{qq}(\omega)$ is the Fourier transform of the correlation function of (6) ($q = x,y,z$) and can be calculated in terms of the Fourier transform of the cross correlation functions (4). These formulas hold if $T_1, T_2 \gg 2\pi/\omega_L$ (secular regime) and T_1, T_2 are longer than the electronic relaxation times (Markov regime). In addition, fluctuations of the three components of $\mathbf{H}_{\rm hyp}$ are assumed independent. The last assumption is not correct when the hyperfine field has a dipolar origin as in the present case. We have calculated the generalized coupled differential equations for the decay of the nuclear magnetization.[38] We have numerically checked that in the experimental conditions of this work it is still possible to decouple the equations as in Redfield's theory and calculate the relaxation rates as in (A3) and (A4). Taking as inputs the positions of the magnetic ions and protons in the molecule, we

can calculate $1/T_1$ and $1/T_2$ for the Fe_7 cluster as

$$\frac{1}{T_1} = \sum_{\substack{i,j=1,N \\ p,p'=x,y,z}} C_{i,j}^{p,p'} \left[\mathcal{S}_{s_i^p, s_j^{p'}}(\omega_L) + \mathcal{S}_{s_i^p, s_j^{p'}}(-\omega_L) \right], \quad \text{(A5)}$$

$$\frac{1}{T_2} = \frac{1}{2T_1} + \sum_{\substack{i,j=1,N \\ p,p'=x,y,z}} K_{i,j}^{p,p'} \left[\mathcal{S}_{s_i^p, s_j^{p'}}(0) \right], \quad \text{(A6)}$$

where the $C_{i,j}^{p,p'}$ and $K_{i,j}^{p,p'}$ are geometric coefficients of the hyperfine dipolar interaction between magnetic ions and protons.[26]

The transverse relaxation rate $1/T_2$ has also a temperature-independent contribution originating from the nuclear dipole-dipole interaction among protons. At high temperatures, the electronic contribution to $1/T_2$ in (A4) is small and only the nuclear dipole-dipole contribution survives. In fact, in the Fe_7 cluster $1/T_2$ is almost temperature independent at $T > 40$ K and thus we can take as a measure of the nuclear dipole-dipole contribution the experimental value of $1/T_2$ at $T = 80$ K.

[1] R. Sessoli, D. Gatteschi, A. Caneschi, and M. A. Novak, Nature (London) **365**, 141 (1993).
[2] L. Bogani and W. Wernsdorfer, Nat. Mater. **7**, 179 (2008).
[3] M. N. Leuenberg and D. Loss, Nature (London) **410**, 789 (2001).
[4] F. Meier, J. Levy, and D. Loss, Phys. Rev. Lett. **90**, 047901 (2003).
[5] F. Troiani, A. Ghirri, M. Affronte, S. Carretta, P. Santini, G. Amoretti, S. Piligkos, G. A. Timco, and R. E. P. Winpenny, Phys. Rev. Lett. **94**, 207208 (2005).
[6] J. Lehman, A. Gaita-Ariño, E. Coronado, and D. Loss, Nature Nanotechnol. **2**, 312 (2007).
[7] M. Affronte, A. Ghirri, S. Carretta, G. Amoretti, S. Piligkos, G. A. Timco, and R. E. P. Winpenny, Appl. Phys. Lett. **84**, 3468 (2004).
[8] M. Evangelisti, A. Candini, M. Affronte, E. Pasca, L. J. de Jongh, R. T. W. Scott, and E. K. Brechin, Phys. Rev. B **79**, 104414 (2009).
[9] J. R. Friedman, M. P. Sarachik, J. Tejada, and R. Ziolo, Phys. Rev. Lett. **76**, 3830 (1996).
[10] L. Thomas, F. Lionti, R. Ballou, D. Gatteschi, R. Sessoli, and B. Barbara, Nature (London) **383**, 145 (1996).
[11] N. V. Prokif'ev and P. C. Stamp, Phys. Rev. Lett. **80**, 57940 (1998).
[12] S. Carretta, P. Santini, G. Amoretti, T. Guidi, J. R. D. Copley, Y. Qiu, R. Caciuffo, G. Timco, and R. E. P. Winpenny, Phys. Rev. Lett. **98**, 167401 (2007).
[13] C. Schlegel, J. van Slageren, M. Manoli, E. K. Brechin, and M. Dressel, Phys. Rev. Lett. **101**, 147203 (2008).
[14] W. Wernsdorfer, N. Aliaga-Alcade, D. N. Hendrickson, and G. Christou, Nature (London) **416**, 406 (2002).
[15] S. Hill, R. S. Edwards, N. Aliaga-Alcade, and G. Christou, Science **302**, 1015 (2003).
[16] G. Timco, S. Carretta, F. Troiani, F. Tuna, R. J. Pritchard, C. A. Muryn, E. J. L. McInnes, A. Ghirri, A. Candini, P. Santini, G. Amoretti, M. Affronte, and R. E. P. Winpenny, Nature Nanotechnol. **4**, 173 (2009).
[17] A. Candini, G. Lorusso, F. Troiani, A. Ghirri, S. Carretta, P. Santini, G. Amoretti, C. Muryn, F. Tuna, G. A. Timco, E. J. L. McInnes, R. E. P. Winpenny, W. Wernsdorfer, and M. Affronte, Phys. Rev. Lett. **104**, 037203 (2010).
[18] D. Gatteschi, R. Sessoli, and J. Villain, *Molecular Nanomagnets* (Oxford University Press, New York, 2006).
[19] J. S. Gardner, M. J. P. Gingras, and J. E. Greedan, Rev. Mod. Phys. **82**, 53 (2010).
[20] T. H. Diep, *Magnetic systems with competing interactions* (World Scientific, Singapore, 1994).
[21] J. Schnack, Dalton Trans. **39**, 4677 (2010).
[22] J. Schnack, R. Schmidt, and J. Richter, Phys. Rev. B **76**, 054413 (2007).
[23] K. Mason, J. Chang, E. Garlatti, A. Prescimone, S. Yoshii, H. Nojiri, J. Schnack, P. A. Tasker, S. Carretta, and E. K. Brechin, Chem. Comm. **47**, 6018 (2011); K. Mason, J. Chang, A. Prescimone, E. Garlatti, S. Carretta, P. A. Tasker, and E. K. Brechin, Dalton Trans. **41**, 8777 (2012).
[24] E. Garlatti, S. Carretta, M. Affronte, E. C. Sañudo, G. Amoretti, and P. Santini, J. Phys.: Condens. Matter **24**, 104006 (2012).
[25] P. Santini, S. Carretta, E. Liviotti, G. Amoretti, P. Carretta, M. Filibian, A. Lascialfari, and E. Micotti, Phys. Rev. Lett. **94**, 077203 (2005).
[26] A. Bianchi, S. Carretta, P. Santini, G. Amoretti, J. Lago, M. Corti, A. Lascialfari, P. Arosio, G. Timco, and R. E. P. Winpenny, Phys. Rev. B **82**, 134403 (2010).
[27] F. Borsa, A. Lascialfari, and Y. Furukawa, in *Novel NMR and EPR Techniques* (Springer, Berlin, Heidelberg, 2006).
[28] M. Belesi, A. Lascialfari, D. Procissi, Z. H. Jang, and F. Borsa, Phys. Rev. B **72**, 014440 (2005).
[29] C. Cañada-Vilalta, T. A. O'Brien, E. K. Brechin, M. Pink, E. R. Davidson, and G. Christou, Inorg. Chem. **43**, 5505 (2004).
[30] S. H. Baek, M. Luban, A. Lascialfari, E. Micotti, Y. Furukawa, F. Borsa, J. van Slageren, and A. Cornia, Phys. Rev. B **70**, 134434 (2004).
[31] S. Carretta, P. Santini, G. Amoretti, M. Affronte, A. Candini, A. Ghirri, I. S. Tidmarsh, R. H. Laye, R. Shaw, and E. J. L. McInnes, Phys. Rev. Lett. **97**, 207201 (2006).
[32] A magnetoelastic coupling with a single site-independent parameter γ leads to a nonergodic spin dynamics. Thus, we have chosen slightly different coupling constants for each Fe^{3+} ion and we have checked that the results don't depend qualitatively on the choice of the specific pattern of coupling constants (Ref. 31).
[33] P. Santini, S. Carretta, E. Liviotti, and G. Amoretti, Physica B **374-375**, 109 (2006).
[34] A. Abragam and B. Bleaney, *Electron Paramagnetic Resonance of Transition Ions* (Clarendon Press, Oxford, 1970).
[35] A. G. Redfield, IBM J. **1**, 19 (1957).
[36] R. K. Wangsness and F. Bloch, Phys. Rev. **89**, 728 (1953).
[37] C. P. Slichter, *Principles of magnetic resonance* (Springer-Verlag, New York, 1992).
[38] E. Garlatti, S. Carretta, P. Santini, and G. Amoretti (unpublished).